Letter

Relaxation at different length scales in models of many-body localization

J. Herbrych[1], M. Mierzejewski,[1] and P. Prelovšek[2,3]

[1]*Department of Theoretical Physics, Faculty of Fundamental Problems of Technology,*
Wrocław University of Science and Technology, 50-370 Wrocław, Poland
[2]*Jožef Stefan Institute, SI-1000 Ljubljana, Slovenia*
[3]*Faculty of Mathematics and Physics, University of Ljubljana, SI-1000 Ljubljana, Slovenia*

We study dynamical correlation functions in the random-field Heisenberg chain, which probes the relaxation times at different length scales. First, we show that the relaxation time associated with the dynamical imbalance (examining the relaxation at the smallest length scale) decreases with disorder much faster than the one determined by the dc conductivity (probing the global response of the system). We argue that the observed dependence of relaxation on the length scale originates from local nonresonant regions. The latter have particularly long relaxation times or remain frozen, allowing for nonzero dc transport via higher-order processes. Based on the numerical evidence, we introduce a toy model that suggests that the nonresonant regions asymptotic dynamics are essential for the proper understanding of the disordered chains with many-body interactions.

Introduction. The phenomenon of many-body localization (MBL) deals with a challenging interplay of disorder [1] and interaction in many-body (MB) quantum systems [2], opening also fundamental questions on the statistical description of such systems. It is suggested by numerous numerical studies that prototype one-dimensional (1D) models on increasing disorder reveal the transition/crossover from an ergodic behavior to a localized regime characterized by several criteria: change in level statistics and spectral properties [3–7], slow growth of entanglement entropy [8–10], vanishing dc conductivities and transport [11–16], nonergodic behavior of local correlations, and the absence of thermalization [17–21], the latter also being the experimental probe in cold-atom systems [22–24]. Recently, due to the restricted system sizes available in the numerical investigations, the stability of the MBL phase has been challenged [25,26]. Nevertheless, even in reachable systems, the transport as well as the relaxation properties are well defined at high temperatures $T = 1/\beta \to \infty$, provided that (i) we consider properties at fixed disorder configuration, and (ii) we take into account that the frequency resolution is limited, i.e., $\delta\omega \gtrsim \omega_H \sim 1/\tau_H$, where τ_H is the Heisenberg time which in considered finite MB systems can be very long $\tau_H \propto 2^L$.

In this work, we study the high-T transport via the dynamical spin conductivity $\sigma(\omega)$, as well as local correlations embodied by the dynamical imbalance $I(\omega)$, and reveal the characteristic relaxation rates at different length scales in the prototype model of MBL, i.e., the 1D random-field Heisenberg model. While it has already been observed that the average dc value $\sigma_0 = \sigma(\omega \to 0)$ depends exponentially on disorder W [12,15,16,27,28], we establish that this is also the property for each disorder configuration. Still, differences of exponent lead to very broad (log-normal type) distribution of σ_0 [27,29] even at modest disorders $W < W_c^*$, where W_c^* is the

value of the presumed MBL crossover/transition $W_c^* \sim 4J$ in the random HM [4,14,17]. On the other hand, the relaxation of local quantities, as manifested in $I(\omega)$ and spatially resolved spin correlations, can reveal very small relaxation rates, which can be below the resolution $\Gamma < \delta\omega$ in considered systems and are an indication of much slower thermalization and approach to ergodicity [6,30]. The observed phenomena can be well captured within a toy model, which separates for each disorder configuration the system into resonant islands [31–33] and nonresonant quasilocalized islands. The transport through the latter can happen via higher-order tunneling while local thermalization occurs on much longer time scales [33,34]. In spite of its simplicity the model accounts well for observed steep decrease of conductivity with disorder and its wide statistical spread. We also find similar transport properties win the random transverse Ising model (TFIM) [35].

Model. In the following we mostly study the random-field Heisenberg model,

$$H = \sum_i \left[\frac{J}{2}(S_{i+1}^+ S_i^- + \text{H.c.}) + J\Delta S_{i+1}^z S_i^z + h_i S_i^z \right], \quad (1)$$

with spin $S = 1/2$ operators and $\Delta = 1$, while $h_i \in [-W, W]$ are local fields with uniform probability distribution. We consider 1D chains with L sites and periodic boundary conditions, with $J = 1$ as the energy unit. We first concentrate on the high-T ($T \gg J$) dynamical spin conductivity,

$$\tilde{\sigma}(\omega) = T\sigma(\omega) = \frac{1}{L} \int_0^\infty dt\, e^{i\omega t} \langle j(t)j \rangle, \quad (2)$$

related to the uniform spin current $j = (J/2)\sum_j(iS_{j+1}^+ S_j^- + \text{H.c.})$. We calculate $\tilde{\sigma}(\omega)$ (and other dynamical correlation functions considered in this work) for each disorder configuration using the upgraded microcanonical Lanczos method
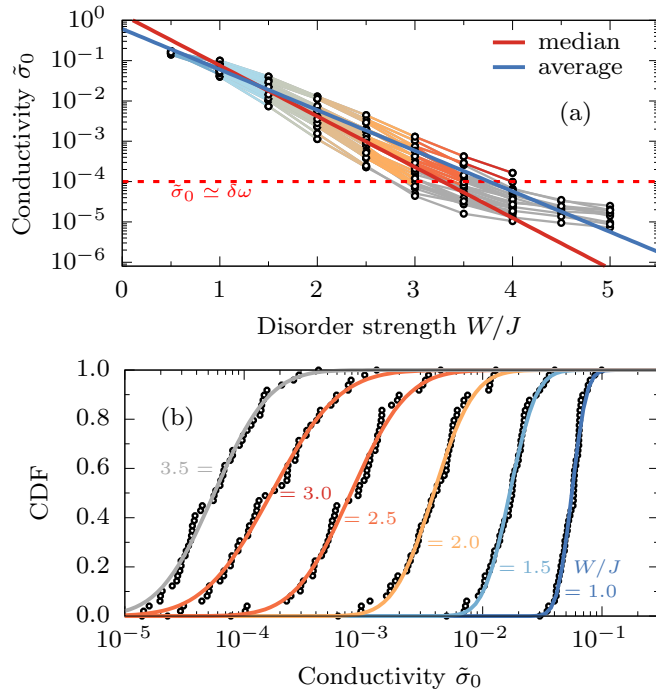
FIG. 1. (a) High-T dc spin conductivities $\tilde{\sigma}_0$ within the random-field Heisenberg model vs disorder strength W for different disorder realizations (30 samples for each W), as evaluated with MCLM on the $L = 26$ system. The thick lines represent exponential fits to the median and average $\tilde{\sigma}_0$. (b) Cumulative distribution function (CDF) of $\tilde{\sigma}_0$ values for different W (50 samples for each W). Curves represent log-normal distributions as a guide to the eye.

(MCLM) [28,36–38] with high-resolution $\delta\omega$. The method evaluates the dynamical correlations within a microcanonical state $|\Psi_\mathcal{E}\rangle$ corresponding to chosen energy $\mathcal{E}$ (which we choose here in the middle of the MB spectrum, i.e., $\mathcal{E} \sim 0$) and with small energy dispersion $\sigma_\mathcal{E} < \delta\omega \sim \Delta E/M_L$, obtained via a large number of Lanczos iterations M_L, where ΔE is the system MB energy span. In the following, we present results for $L = 26$ sites in the $S_{\text{tot}}^z = 0$ sector, with the number of MB states $N_{st} \sim 10^7$ states, and by using $M_L \sim 2.10^5$ we reach (in considered disorder range $W \leqslant 4$) the resolution $\delta\omega \sim 10^{-4}$, still larger than $\omega_H \sim \Delta E/N_{st} \lesssim 10^{-5}$.

It should be noted that even within a finite system for chosen sample h_i and energy $\mathcal{E}$ dynamical $\tilde{\sigma}(\omega)$, and in particular $\tilde{\sigma}_0$, are well defined and resolved provided that $\tilde{\sigma}_0 \gtrsim \delta\omega$ (see Ref. [35] for typical spectra $\tilde{\sigma}(\omega)$ at different W). In Fig. 1(a) we summarize results for dc $\tilde{\sigma}_0$ at increasing W, where we choose $h_i = W\eta_i$ with random configurations $\eta_i \in [-1, 1]$. We note that $W \sim 1$ roughly represents [35] the borderline between the weak scattering regime and the incoherent diffusion where $\sigma(\omega)$ is maximum at $\omega > 0$. Results in Fig. 1(a) generally reveal for $W > 1$ an exponential-like dependence $\tilde{\sigma}_0 \propto \exp(-bW)$ for each disorder configuration separately, with typical $b \sim 2.5$ [12,15,16,27]. Still, slightly different (sample dependent) b lead to a large statistical spread of $\tilde{\sigma}_0$ value, as summarized in Fig. 1(b) by the cumulative distribution function (CDF) which is close to the log-normal distribution. We also note that our $\delta\omega$ resolution limits reliable $\tilde{\sigma}_0 \gtrsim 10^{-4}$ for different samples at marginal $W_c^* \sim 4$, with the variation $\delta W_c^* \sim 0.5$.
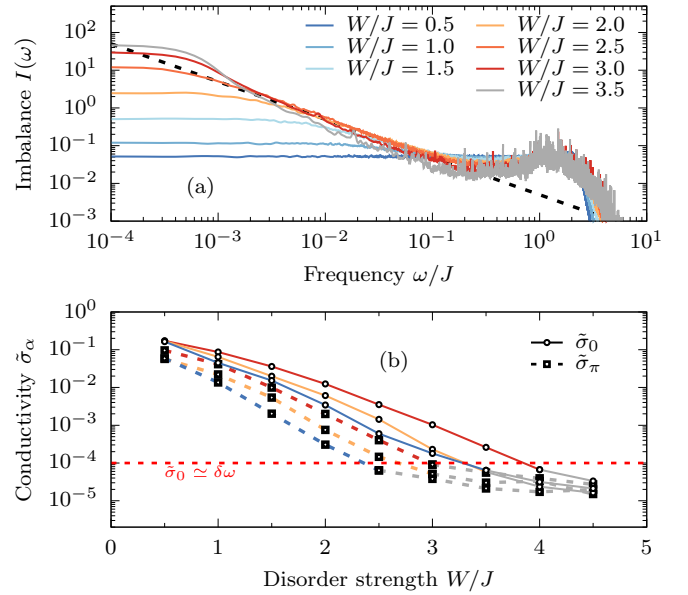

FIG. 2. (a) Dynamical imbalance $I(\omega)$ within a single disorder sample at different strength W, calculated for $L = 26$. Dashed line depicts the $1/\omega$ dependence. (b) Extracted dc spin conductivity $\tilde{\sigma}_\pi$ in comparison with the uniform $\tilde{\sigma}_0$ vs W for three potential configurations.

In contrast to $\tilde{\sigma}_0$, which can be typically well followed for $W \lesssim 3.5$, local correlations can reveal already exceedingly long relaxation times. Of interest is the spin correlations $S_q(\omega)$ of modulation operator $S_q^z = (1/\sqrt{L}) \sum_j \exp(iqj)S_j^z$ which can be related [16,21,35,39,40] to the q-dependent spin conductivity $\tilde{\sigma}_q$

$$S_q(\omega) = -\frac{1}{\pi}\text{Im}\left[\frac{\chi_q^0}{\omega + i\, g_q^2 \tilde{\sigma}_q(\omega)/\chi_q^0}\right]. \qquad (3)$$

Here $g_q = 2\sin(q/2)$ and $\chi_q^0 = \langle S_{-q}^z S_q^z \rangle = 1/4$. Note also that $S_\pi(\omega) = I(\omega)$ is directly relevant to cold-atom experiments [22–24], i.e., $I(\omega)$ probes the local thermalization, in particular the relaxation rate $\Gamma_I \propto \tilde{\sigma}_\pi(\omega \to 0) = \tilde{\sigma}_\pi$, determined by the saturation $I(\omega < \Gamma_I) \propto 1/\sigma_\pi$. Results in Fig. 2(a) for a single disorder configuration reveal that Γ_I can become very small and hardly resolved in the considered system, i.e., $\Gamma_I \lesssim \delta\omega$, even at modest $W \sim 2.5$, where $\tilde{\sigma}_0$ is still well defined. An indication of finite-size dominated Γ_I is also the deviation from marginal $I(\omega) \propto 1/\omega$ [16,21] at larger $W \lesssim W_c^*$. Furthermore, the results for $\tilde{\sigma}_\pi$ extracted from $I(\omega)$ for a few samples are presented in Fig. 2(b) and confirm that in general $\tilde{\sigma}_\pi < \tilde{\sigma}_0$, with the difference becoming large on approaching $W \sim W_c^*$, i.e., indicated increasing difference between thermalization and (local) transport relaxation.

While $I(\omega)$ and related Γ_I monitor the local relaxation averaged over all sites in the system, it is instructive to follow also the local $C_i(\omega)$, i.e., correlations of S_i^z for each site in the chain. In Fig. 3(a) we present a variation of $C_i(\omega)$ among all sites in one chosen configuration at moderate $W = 3$. We note substantial variations in low-frequency $C_i(\omega \to 0) \propto 1/\Gamma_i$, whereby small Γ_i can be directly correlated with large potential deviations of local h_i, also presented in Fig. 3(a).
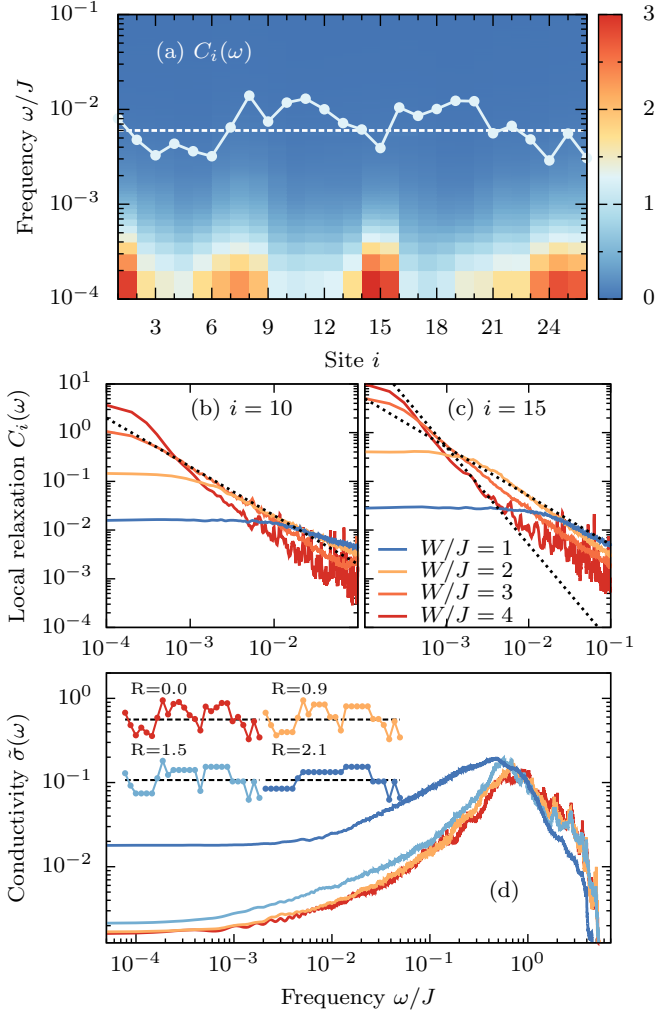
FIG. 3. (a) Local spin correlations $C_i(\omega)$ for all sites $i = 1, L$ with potentials h_i corresponding to $W = 3$ (with the potential landscape also shown). (b), (c) Local correlations $C_i(\omega)$ for different $W = 1-3$ for two characteristic sites $i = 10, 15$, representing resonant and localized islands, respectively. Dashed line in (b) represent $\propto 1/\omega$ dependence, while in (c) $\propto 1/\omega$ and $\propto 1/\omega^2$. (d) $\tilde{\sigma}(\omega)$ for flattened potentials with various thresholds $R = 0 - 2.1$ for one configuration with $W = 3$.

A more detailed comparison of $C_i(\omega)$ for two typical sites, representing the weak potential fluctuation, site $i = 10$, and strong potential-fluctuation regime at $i = 15$, respectively, are shown in Figs. 3(b) and 3(c). While generally $C_{15}(\omega \sim 0) \gg C_{10}(\omega \sim 0)$, it also appears that $C_{15}(\omega)$ reveals for $W \geqslant 3$ [instead of $C_i(\omega > \Gamma_i) \propto 1/\omega$] a Lorentzian behavior [30] with $C_i(\omega > \Gamma_i) \propto 1/\omega^2$, representing the marginal $\Gamma_i \sim \delta\omega$. It follows from Fig. 3(a) that the local dynamics captured in $C_i(\omega)$ is particularly slow in the vicinity of sites i with a large difference in local potentials $|h_i - h_{i\pm1}|$. One could in fact expect for the latter a Lorentzian with $\Gamma_i \propto \exp(-a|h_i|)$, with large $a > 3$ [33]. While we simulate such a case in Ref. [35], we find much smaller $a \sim 1$, which can better account for observed differences in Γ_i.

As the main result we demonstrate that the regions with slow dynamics are essential not only for thermalization of local operators but also for transport at various length scales,

i.e., $\tilde{\sigma}_0$ vs $\tilde{\sigma}_\pi$, and various time scales. We introduce a parameter R which allows us to distinguish between the *nonresonant (localized)* islands and the *resonant (conducting)* islands. Namely, we assume that site i belongs to an isolated island when $|h_i - h_j| > R$ for both neighboring sites, $j = i \pm 1$. Otherwise, i belongs to a conducting island. We note that taking the standard resonant scenario [28,32], together with the matrix elements relevant for the spin-flip $J/2$, one gets $R = J = 1$. Interestingly, we observe that the spatial variation of h_i within the conducting islands is not essential for transport. To this end, for all sites i which belong to the conducting islands we replace h_i with $\bar{h}_i$, where $\bar{h}_i$ is the average h_j over all sites j in the same island. Such flattening eliminates disorder within each conducting island, as is sketched in Fig. 3(d) for a single configuration at $W = 3$. We notice from Fig. 3(d) that the resulting $\tilde{\sigma}(\omega)$ is hardly affected up to $R \simeq 1.5$. This result reveals a clear separation of the studied system into conducting and localized islands, and shows that the transport is determined by the localized islands.

Toy model. Since the time scales which are relevant for the dynamics in the conducting and isolated islands differ substantially, the latter can be considered to be frozen and transformed out from the Hamiltonian. Then, the transport through a localized island that contains M frozen spins, $S_j^z \cdots S_{j+M-1}^z$, can happen via high-order virtual process involving at least M spin flips. It leads to a new effective spin-flip term, $\tilde{H}_j' = (J_{j+M}^{\text{eff}}/2)(S_{j+M}^+ S_{j-1}^- + \text{H.c})$, between sites $j - 1$ and $j + M$, which belong to the neighboring conducting islands [33]. One can derive J_j^{eff} via the Mth order degenerate perturbation theory

$$\tilde{H}_j' = H'Q\frac{1}{\bar{E} - H_0}H'Q \cdots QH'\frac{1}{\bar{E} - H_0}QH', \quad (4)$$

where $H_0 = H_h + H_\Delta$ and Q projects all intermediate states equal to the initial or the final ones. Here, H', H_Δ, and H_h denote, respectively, the first, second, and last term in the Hamiltonian (1). In order to obtain an analytical estimate for J_j^{eff}, we introduce a few simplifications. We assume strong disorder ($H_0 \simeq H_h$) ferromagnetic states of isolated islands ($S_i^z = S_{i'}^z$ for $i, i' = j, ..., j + M - 1$), and we fix $\bar{E} = (E_i + E_f)/2$ as the average between initial and final H_h, taking also $\bar{h}_{j-1} \sim \bar{h}_{j+M} \sim 0$. Then, one can directly evaluate Eq. (4) and the effective coupling

$$\left|J_j^{\text{eff}}\right| = \frac{J^{M+1}}{2^M}\frac{1}{h_j h_{j+1} \cdots h_{j+M-1}}. \quad (5)$$

It is interesting to note that Eq. (4) remains valid for other spin configurations apart from ferromagnetic, which we have checked explicitly for $M \leqslant 3$.

It is now straightforward to define a toy model which relies on the assumption that dc transport is dominated by the *incoherent* conduction via localized islands. Then, the transport appears through the sequence of incoherent hoppings (series of resistors), i.e., corresponding to $J_i = J$ for the link in the resonant islands and $J_i = J_j^{\text{eff}}/M$ for each link in the nonresonant ones. Under such conditions, the conductivity is given by $\tilde{\sigma}_0 \sim \sigma_0^* \bar{J}^{\text{eff}}$ and $1/\bar{J}^{\text{eff}} = (1/L)\sum_i (J_i)^{-1}$ where the numerical constant $\sigma_0^* \sim 0.1$ is chosen to reproduce the incoherent dc conductivity at $W \sim 1$. The perturbative expression, Eq. (5), is applicable for realizations of disorder where
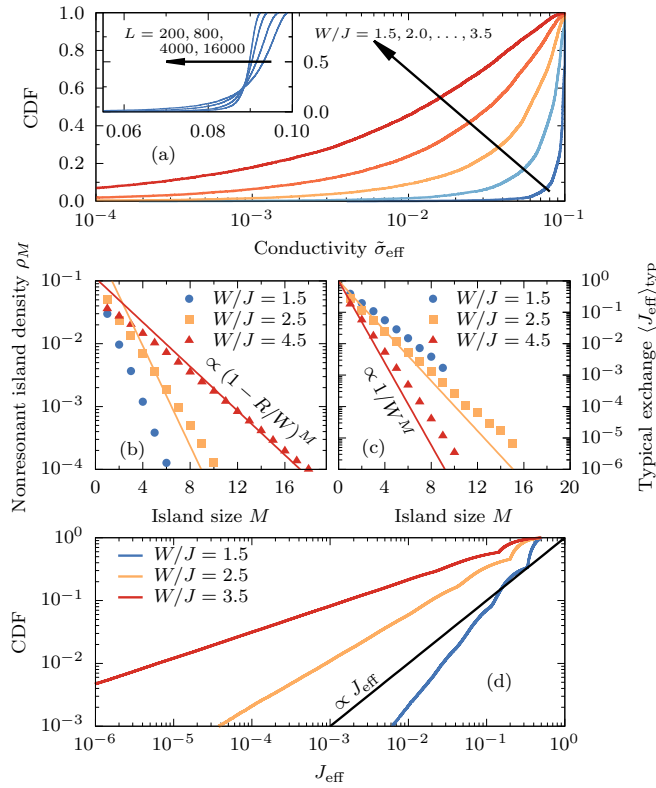
FIG. 4. (a) Toy-model dc conductivity $\tilde{\sigma}_0$ for various W and $L = 25$. The inset show $L = 20$–16000 dependence for $W = 1.5$. (b),(c) Density ρ_M and typical value of J^{eff} for nonresonant islands of length M obtained for $L = 10^7$. (d) Distribution of J^{eff} in the toy model.

potentials inside the island are not degenerate with the outside ones, i.e., $|h_i| \gg 0$. In order to account for the latter, we neglect localized islands with M sites for which $J_i^{\mathrm{eff}} > J/M$.

We have carried out simulations of the toy model following all steps previously tested via full quantum calculations. For each realization of disorder we identify the resonant and nonresonant islands, flatten the disorder within the resonant islands ($h_i \to \bar{h}_i$) and evaluate $\tilde{\sigma}_0$. Based on results shown in Fig. 3(d) we take $R = 1.5$. The main panel in Fig. 4(a) shows the CDF of $\tilde{\sigma}_0$ obtained for different disorder realizations. The toy model correctly reproduces the main features of the full-quantum calculations. In particular, the median of the CDF decays approximately exponentially with W, however the rate is slower than results shown in Fig. 1(b). Moreover, the distribution of $\tilde{\sigma}_0$ for $L \sim 25$ is very broad indicating that the spread of $\tilde{\sigma}_0$ may span over a few orders of magnitude. For weak disorder, the width of the distribution decreases with L, and for sufficiently large systems the distribution approaches the normal (Gaussian) distribution expected for diffusive systems, as shown in the inset of Fig. 4(a).

For stronger disorder, the toy model reveals an anomalous Griffiths scenario reported in several numerical studies [13,41,42]. To explain its origin, in Fig. 4(b) we show the density of nonresonant islands of length M, $\rho_M = N_M/L$, where N_M denotes the number of localized islands and the simulations were carried out for $L = 10^7$. The probability of

finding a nonresonant link in strongly disordered system is $(1 - R/W)$, hence $\rho_M \propto (1 - R/W)^M$. Figure 4(c) shows the typical value of J_{eff} for nonresonant islands of length M. We find $\langle J_{\mathrm{eff}} \rangle_{\mathrm{typ}} \propto W^{-M}$, which straightforwardly follows from Eq. (5). The exponential dependence of ρ_M and $J_{\mathrm{eff}}(M)$ on M is very robust. As a consequence, the toy model realizes the Griffiths scenario, i.e., large nonersonant islands are exponentially rare but the corresponding $1/J_{\mathrm{eff}}$ is exponentially large. Consequently, such islands have a substantial impact on transport. The interplay leads to a power-law CDF $\propto J_{\mathrm{eff}}^{\alpha}$ shown in Fig. 4(d). The probability density $f(J_{\mathrm{eff}}) \propto J_{\mathrm{eff}}^{(\alpha-1)}$ and the average $\langle J_{\mathrm{eff}}^{-1} \rangle = \int_0^1 dJ f(J)/J$ is finite only for $\alpha > 1$ and diverges otherwise. The latter implies $\tilde{\sigma}_0 \to 0$ in the $L \to \infty$ limit, indicating subdiffusive transport or localization. It should be stressed that the toy model is based on the assumption that the nonresonant islands are strictly frozen. If the lifetimes are finite, then the nondiffusive transport may be transient while the asymptotic transport may still be diffusive. It is also possible that the role of large islands may be over represented due to possible inherent internal resonances. Results in Fig. 3(c) indicate that the relaxation of the nonresonant islands can be studied numerically only up to relatively weak disorder $W \simeq 2.5$.

Conclusions. We have studied dynamical correlation functions which probe the relaxation mechanisms at different length scales in the random-field Heisenberg model. The dc conductivity $\tilde{\sigma}_0$ probes the transport at large length scales (wave vectors $q \to 0$) and was shown to decrease exponentially with disorder with an increasing log-normal-like distribution of $\tilde{\sigma}_0$ values. Still, its decrease disorder is much slower than the dynamical imbalance and the corresponding $\tilde{\sigma}_\pi$, which probes the smallest length scales ($q = \pi$). We argue that the surprising difference between $\tilde{\sigma}_0$ and $\tilde{\sigma}_\pi$ originates from the presence of nonresonant regions (islands) with particularly slow or completely frozen dynamics. These extremely long (or infinite) relaxation times are probed by the long-time dynamics of the imbalance or, equivalently, by $\tilde{\sigma}_\pi(\omega \to 0)$. However, their contribution to $\tilde{\sigma}_0$ can be treated perturbatively in that spins excitation can pass nonresonant islands via virtual spin-flip processes (on the much shorter time scales). As a consequence the nonresonant islands influence $\tilde{\sigma}_\pi$ more strongly than $\tilde{\sigma}_0$. Still, the presence of nonresonant islands explains large sample-to-sample spread of $\tilde{\sigma}_0$ and the exponential dependance of $\tilde{\sigma}_0$ on the strength of disorder. Large nonresonant islands may also give rise to anomalous (nondiffusive) transport for stronger disorder, although their role can be overestimated in the present study. It is evident from the presented results that the fate of the MBL phase and transport properties of the disorder many-body systems depends on the relaxation times of the nonresonant islands, i.e., whether the latter are finite or infinite.

[1] P. W. Anderson, Absence of diffusion in certain random lattices, Phys. Rev. **109**, 1492 (1958).

[2] D. M. Basko, I. L. Aleiner, and B. L. Altshuler, Metal–insulator transition in a weakly interacting many-electron system with localized single-particle states, Ann. Phys. (NY) **321**, 1126 (2006).

[3] V. Oganesyan and D. A. Huse, Localization of interacting fermions at high temperature, Phys. Rev. B **75**, 155111 (2007).

[4] D. J. Luitz, N. Laflorencie, and F. Alet, Many-body localization edge in the random-field Heisenberg chain, Phys. Rev. B **91**, 081103(R) (2015).

[5] M. Serbyn and J. E. Moore, Spectral statistics across the many-body localization transition, Phys. Rev. B **93**, 041424(R) (2016).

[6] J. Šuntajs, J. Bonča, T. Prosen, and L. Vidmar, Quantum chaos challenges many-body localization, Phys. Rev. E **102**, 062144 (2020).

[7] P. Sierant, D. Delande, and J. Zakrzewski, Thouless Time Analysis of Anderson And Many-Body Localization Transitions, Phys. Rev. Lett. **124**, 186601 (2020).

[8] M. Žnidarič, T. Prosen, and P. Prelovšek, Many-body localization in the heisenberg XXZ magnet in a random field, Phys. Rev. B **77**, 064426 (2008).

[9] J. H. Bardarson, F. Pollmann, and J. E. Moore, Unbounded Growth of Entanglement in Models of Many-Body Localization, Phys. Rev. Lett. **109**, 017202 (2012).

[10] M. Serbyn, Z. Papić, and D. A. Abanin, Criterion for Many-Body Localization-Delocalization Phase Transition, Phys. Rev. X **5**, 041047 (2015).

[11] T. C. Berkelbach and D. R. Reichman, Conductivity of disordered quantum lattice models at infinite temperature: Many-body localization, Phys. Rev. B **81**, 224429 (2010).

[12] O. S. Barišić and P. Prelovšek, Conductivity in a disordered one-dimensional system of interacting fermions, Phys. Rev. B **82**, 161106(R) (2010).

[13] K. Agarwal, S. Gopalakrishnan, M. Knap, M. Müller, and E. Demler, Anomalous Diffusion and Griffiths Effects Near the Many-Body Localization Transition, Phys. Rev. Lett. **114**, 160401 (2015).

[14] Y. Bar Lev, G. Cohen, and D. R. Reichman, Absence of Diffusion in an Interacting System of Spinless Fermions on a One-Dimensional Disordered Lattice, Phys. Rev. Lett. **114**, 100601 (2015).

[15] R. Steinigeweg, J. Herbrych, F. Pollmann, and W. Brenig, Scaling of the optical conductivity in the transition from thermal to many-body localized phases, Phys. Rev. B **94**, 180401(R) (2016).

[16] P. Prelovšek, M. Mierzejewski, O. Barišić, and J. Herbrych, Density correlations and transport in models of many-body localization, Ann. Phys. (Berlin) **529**, 1600362 (2017).

[17] A. Pal and D. A. Huse, Many-body localization phase transition, Phys. Rev. B **82**, 174411 (2010).

[18] M. Serbyn, Z. Papić, and D. A. Abanin, Local Conservation Laws and the Structure of the Many-Body Localized States, Phys. Rev. Lett. **111**, 127201 (2013).

[19] D. A. Huse, R. Nandkishore, and V. Oganesyan, Phenomenology of fully many-body-localized systems, Phys. Rev. B **90**, 174202 (2014).

[20] D. J. Luitz, N. Laflorencie, and F. Alet, Extended slow dynamical regime prefiguring the many-body localization transition, Phys. Rev. B **93**, 060201(R) (2016).

[21] M. Mierzejewski, J. Herbrych, and P. Prelovšek, Universal dynamics of density correlations at the transition to many-body localized state, Phys. Rev. B **94**, 224207 (2016).

[22] M. Schreiber, S. S. Hodgman, P. Bordia, H. P. Lüschen, M. H. Fischer, R. Vosk, E. Altman, U. Schneider, and I. Bloch, Observation of many-body localization of interacting fermions in a quasi-random optical lattice, Science **349**, 842 (2015).

[23] S. S. Kondov, W. R. McGehee, W. Xu, and B. DeMarco, Disorder-Induced Localization in a Strongly Correlated Atomic Hubbard Gas, Phys. Rev. Lett. **114**, 083002 (2015).

[24] H. P. Lüschen, P. Bordia, S. Scherg, F. Alet, E. Altman, U. Schneider, and I. Bloch, Observation of Slow Dynamics near the Many-Body Localization Transition in One-Dimensional Quasiperiodic Systems, Phys. Rev. Lett. **119**, 260401 (2017).

[25] S. Bera, G. De Tomasi, F. Weiner, and F. Evers, Density Propagator for Many-Body Localization: Finite-Size Effects, Transient Subdiffusion, and Exponential Decay, Phys. Rev. Lett. **118**, 196801 (2017).

[26] R. K. Panda, A. Scardicchio, M. Schulz, S. R. Taylor, and M. Žnidarič, Can we study the many-body localisation transition? EPL (Europhysics Letters) **128**, 67003 (2020).

[27] O. S. Barišić, J. Kokalj, I. Balog, and P. Prelovšek, Dynamical conductivity and its fluctuations along the crossover to many-body localization, Phys. Rev. B **94**, 045126 (2016).

[28] P. Prelovšek, M. Mierzejewski, and J. Herbrych, Coexistence of diffusive and ballistic transport in integrable quantum lattice models, Phys. Rev. B **104**, 115163 (2021).

[29] P. Prelovšek, M. Mierzejewski, J. Krsnik, and O. S. Barišić, Many-body localization as a percolation phenomenon, Phys. Rev. B **103**, 045139 (2021).

[30] L. Vidmar, B. Krajewski, J. Bonča, and M. Mierzejewski, Phenomenology of Spectral Functions in Disordered Spin Chains at Infinite Temperature, Phys. Rev. Lett. **127**, 230603 (2021)

[31] T. Thiery, F. Huveneers, M. Müller, and W. De Roeck, Many-Body Delocalization as a Quantum Avalanche, Phys. Rev. Lett. **121**, 140601 (2018).

[32] P. Prelovšek, O. S. Barišić, and M. Mierzejewski, Reduced-basis approach to many-body localization, Phys. Rev. B **97**, 035104 (2018).

[33] D. Sels and A. Polkovnikov, Thermalization of dilute impurities in one dimensional spin chains, arXiv:2105.09348.

[34] P. Sierant and J. Zakrzewski, Can we observe the many-body localization? arXiv:2109.13608.

[35] See Supplemental Material at http://link.aps.org/supplemental/10.1103/PhysRevB.105.L081105 for additional results for the dynamical conductivity, imbalance, local spin correlations, and random transverse-field Ising model.

[36] M. W. Long, P. Prelovšek, S. El Shawish, J. Karadamoglou, and X. Zotos, Finite-temperature dynamical correlations using the microcanonical ensemble and the Lanczos algorithm, Phys. Rev. B **68**, 235106 (2003).

[37] A. Karahalios, A. Metavitsiadis, X. Zotos, A. Gorczyca, and P. Prelovšek, Finite-temperature transport in disordered Heisenberg chains, Phys. Rev. B **79**, 024425 (2009).

[38] P. Prelovšek and J. Bonča, Ground state and finite temperature lanczos methods, in *Strongly Correlated Systems - Numerical*

Methods, edited by A. Avella and F. Mancini (Springer, Berlin, 2013).

[39] J. Herbrych, R. Steinigeweg, and P. Prelovšek, Spin hydrodynamics in the $s = \frac{1}{2}$ anisotropic Heisenberg chain, Phys. Rev. B **86**, 115106 (2012).

[40] P. Prelovšek and J. Herbrych, Self-consistent approach to many-body localization and subdiffusion, Phys. Rev. B **96**, 035130 (2017).

[41] S. Gopalakrishnan, K. Agarwal, E. A. Demler, D. A. Huse, and M. Knap, Griffiths effects and slow dynamics in nearly many-body localized systems, Phys. Rev. B **93**, 134206 (2016).

[42] M. Mierzejewski, M. Środa, J. Herbrych, and P. Prelovšek, Resistivity and its fluctuations in disordered many-body systems: From chains to planes, Phys. Rev. B **102**, 161111(R) (2020).